An optimized, sensitive and stable reduced graphene oxide–gold nanoparticle-luminol-H_2O_2 chemiluminescence system and its potential analytical application*

Wang Wen-Shuo(王闻硕)[a], He Da-Wei(何大伟)[a]†, Wang Ji-Hong(王继红)[b], Duan Jia-Hua(段嘉华)[a], Peng Hong-Shang(彭洪尚)[a], Wu Hong-Peng(吴洪鹏)[a], Fu Ming(富 鸣)[a], Wang Yong-Sheng(王永生)[a], and Zhang Xi-Qing(张希清)[a]‡

[a] *Key Laboratory of Luminescence and Optical Information, Ministry of Education, Institute of Optoelectronic Technology, Beijing Jiaotong University, Beijing* 100044, *China*

[b] *School of Science, China University of Petroleum, Beijing* 102249, *China*

(Received 12 September 2013; revised manuscript received 30 October 2013; published online 20 February 2014)

The chemiluminescence (CL) performance of luminol is improved using reduced graphene oxide/gold nanoparticle (rGO–AuNP) nano-composites as catalyst. To prepare this catalyst, we propose a linker free, one-step method to *in-situ* synthesize rGO–AuNP nano-composites. Various measurements are utilized to characterize the resulting rGO–AuNP samples, and it is revealed that rGO could improve the stability and conductivity. Furthermore, we investigate the CL signals of luminal catalyzed by rGO–AuNP. Afterwards, the size effect of particle and the assisted enhancement effect of rGO are studied and discussed in detail. Based on the discussion, an optimal, sensitive and stable rGO–AuNP-luminon–H_2O_2 CL system is proposed. Finally, we utilize the system as a sensor to detect hydrogen peroxide and organic compounds containing amino, hydroxyl, or thiol groups. The CL system might provide a more attractive platform for various analytical devices with CL detection in the field of biosensors, bioassays, and immunosensors.

Keywords: graphene, nanoparticles, chemiluminescence, biosensers

PACS: 81.05.ue, 78.67.Bf, 78.60.Ps, 87.85.fk **DOI:** 10.1088/1674-1056/23/4/048103

1. Introduction

With the rapid development of electronic technology and the invention of highly sensitive photomultiplier tubes, chemiluminescence (CL) phenomenon has attracted great attention in quantitative analysis fields such as chemical analysis,[1] environmental science,[2] life science,[3] medicine,[4] etc. Compared with other luminescence methods, CL has a lot of advantages involving no need of external light source and no interference from Rayleigh scattering or Raman scattering. At the same time, it circumvents signal fluctuation caused by light source instability. Due to all these unique properties, CL can greatly improve the signal-to-noise ratio, and thus it is widely used in the areas of biological analysis.

In recent years, considerable work has been devoted to noble nanoparticles-catalyzed CL reactions, especially gold nanostructures.[5–8] For the nanosized metallic particles, the large surface area affords abundant unsaturated/reactive surface atom resulting from dangling bonds, surface steps, wrinkles or defects,[9–13] and yields high catalytic activity consequently. In addition, gold nanoparticles have good biocompatibility and the formation of Au–S bond or Au–N bond is useful for biosencing. For example, Tian *et al.*[14] have reported on the immunosensor based on luminol functionalized gold nanoparticles and Li *et al.*[15] have proposed the aminothiols sensor based on triangular gold nanoparticle-catalyzed luminol chemiluminescence.

Graphene is an ideal solid substrate due to its high mechanic strength as well as unique physical properties such as large surface area.[16] Particularly, reduced graphene oxide (GO) displays high electronic conductivity.[17,18] Therefore, graphene–metal NPs nanocomposites might exhibit better performance in electrochemical detection,[19–21] surface enhanced Raman scattering,[22,23] and two-photon excitation,[24] because of the combination of localized surface plasmon resonance (LSPR) of AuNPs with the fast electron mobility of graphene. To the best of our knowledge, however, there has been no report about reduced graphene oxide/gold nanoparticle (rGO–AuNP) composites as catalysts for CL to date.

In the present work, we propose a linker free, one-step chemical nucleation strategy to synthesize rGO–AuNP nanocomposites. The composites are characterized by atomic force microscope (AFM), Raman spectroscopy, X-ray photoelectron spectroscopy (XPS), UV-Vis absorption spectra, scanning electron microscope (SEM), energy-dispersive spectroscopy (EDS), and electrochemical impedance spectroscopy (EIS). Thereafter, catalytic performance of the nanocomposites is in-

*Project supported by the National Key Basic Research Program, China (Grant Nos. 2011CB932700 and 2011CB932703), the National Natural Science Foundation of China (Grant Nos. 61378073, 61335006, 91123025, and 61077044), and the Beijing Natural Science Fund Project, China (Grant No. 4132031).

†Corresponding author. E-mail: dwhe@bjtu.edu.cn

‡Corresponding author. E-mail: xqzhang@bjtu.edu.cn

© 2014 Chinese Physical Society and IOP Publishing Ltd

vestigated in a luminon–H_2O_2 CL system. The composites exhibit better CL catalytic activity than AuNP. Moreover, size effect of AuNPs and the enhancement of rGO on CL are studied respectively, and possible mechanisms are proposed. Taking advantage of the optimized rGO–AuNP-luminon–H_2O_2 CL system, trace amount of hydrogen peroxide is detected.

2. Experimental section

2.1. Chemicals and solutions

A 0.01-mol/L stock solution of luminol was prepared by dissolving luminol (Sigma) in 0.1-mol/L NaOH solution without further purification. Luminol stock solution was diluted to 2 μM by buffer solutions (CO_3^{2-}/HCO_3^-). Working solution of H_2O_2 was prepared freshly from hydrogen peroxide 30%. A 1%(w/w) $HAuCl_4$ stock solution was prepared by dissolving 1 g of $HAuCl_4{\cdot}3H_2O$ (Shanghai Reagent) in 100-mL water and stored at 4 °C. A 38.8-mM trisodium citrate ($Na_3C_6O_7$) solution was prepared by dissolving trisodium citrate solids in water. All reagents were of analytical grade, and deionized water was used throughout from Aquapro ED12-3002-U system. No specifically mentioned chemicals were purchased from Sinopharm Chemical Reagent (Beijing, China).

2.2. Chemical exfoliation of graphite

The method of graphite exfoliation used here was mainly based on the idea of Hummers and Offeman, and extensively described elsewhere.[25,26] The surfaces of graphite oxide sheets were highly oxygenated, so bearing hydroxyl epoxide, diol, ketone, and carboxyl functional groups could change the van der Waals interactions significantly and lead to a range of solubility in water. The as-prepared solution was dried by lyophilization after ultrasonication and centrifugation. The obtained powder was referred to as GO, and was re-dissolved in water to form a 2-mg·mL^{-1} GO suspension.

2.3. Synthesis of rGO–AuNP nano-composites

The nano-composites were synthesized by the direct reduction of $AuCl_4^-$ in the presence of GO. In a typical experiment, 1-mL GO suspension and 500-μL $HAuCl_4$ solutions were added into 50-mL water. Then the mixture was dispersed adequately by ultrasonication. The resulting suspension was aged for 30 min to promote the interaction of gold ions with the graphene oxide sheet surface. Then the suspension was heated up to 80 °C in a water bath, followed by dropwise addition of 1000 μL of sodium citrate. After reaction for 1 h, the resulting nano-composites were rGO–AuNP nanocomposites. Size of AuNP could be varied by changing the ratio of sodium citrate to $HAuCL_4$. For comparison, pure AuNP was prepared by chemical reduction of $HAuCl_4$ by sodium citrate. The rGO–AuNP and pure AuNP were stored for 24 h at 4 °C.

2.4. Instrumentations and measurements

AFM images were obtained using SPA-300HV (SEIKO, Japan), tapping-mode applied to provide many structural details. Raman spectra were recorded using a Renishaw micro-Raman system with an excitation wavelength of 514 nm. XPS analysis was carried on a PHI Quantera (PHI, Japan). UV-visible spectra, SEM images, and EDS analysis were measured on UV-310IPC spectrometer (Shimadzu, Japan), S4800 microscope (Hitachi, Japan) and EMAX 250 (Horiba, Japan). EIS experiments were performed in the presence of 10-mmol·L^{-1} $K_3Fe(CN)_6$ and 1-mol·L^{-1} KCl as the redox probe, using a CHI660D electrochemical workstation (Chenhua, China). A conventional three-electrode cell was used, including a glassy carbon electrode, a platinum wire, and a saturated calomel electrode.

The CL reactions were carried out in a 3-mL quartz cuvette, and the signals were recorded with an LS 55 fluorescence spectrometer (Perkin Elmer, America). In a typical experiment, 500 μL of luminol solution (2 μM) and 5-μL H_2O_2 (30%) were added to the cuvette sequentially by a pipette. Then, 300-μL rGO–AuNP was injected quickly. The CL signals were displayed and integrated for a 0.5-s interval.

3. Results and discussion

3.1. Characterization of GO

The unique properties of graphene originate from the monolayer honeycomb crystal lattice sheet. It has been reported that bi-layer or tri-layer graphene and their derivative have distinct features in electrical conductivity or mechanical flexibility compared with monolayer.[27] Therefore, identification of single-layer GO from multilayer GO is a crucial step for its future application. The average thickness value of the as-prepared GO sheets is about 0.85 nm with tapping mode AFM (Fig. 1(a)), which is consistent with the typical 0.8-nm thickness value of the monolayer GO reported before.[28] GO is thicker than nonfunctionalized graphene (0.35 nm) due to the existence of oxygenic functional groups on both sides of the sheets.[29] So it can be concluded that most GO sheets are monolayer. The abnormally low or high thickness value of GO sheet is due to the overlaps and defects.

In order to investigate the functional groups on GO sheets, Raman and FTIR spectra are employed here. As shown in Fig. 1(b), the GO sheet exhibits a peak at around 1580 cm^{-1}(G band) corresponding to the E_{2g} photon of C sp^2 atom in a two-dimensional hexagonal lattice. The peak at ca. 1330 cm^{-1} (D band) corresponds to a breathing mode of κ-point phonons of A_{1g} symmetry.[30] It should be noted that the second-order zone boundary phonon (2D band) is not as high as monolayer graphene prepared by other methods (such as chemical vapor deposition and mechanical exfoliation). The reason is mainly due to defects and surface oxygenic functional groups.[31] The

presence of surface oxygenic functional groups is revealed by FTIR spectrum as shown in Fig. 1(c). The absorption bands at 1727 cm^{-1}, 1225cm^{-1}, 1070 cm^{-1}, 1620 cm^{-1} can be attributed to C=O carbonyl stretching vibrations, C–OH hydroxyl stretching, C–O–C ether bond stretching, and the C=C peak respectively.[32] The Raman and FTIR spectra indicate the in-plane sp^2 domains, a partially ordered crystal structure of GO, and the presence of defects and surface oxygenic functional groups.

Surface oxygenic functional groups in GO and rGO are characterized by C1s XPS. The result demonstrates that there are a large number of functional groups on the surface of GO (Fig. 1(d)). In comparison with the spectrum of GO, the spectrum of rGO as shown in Fig. 1(e) exhibits a decreased intensity in the peak of the C–O group, revealing that part of the oxygenic functional groups are reduced.

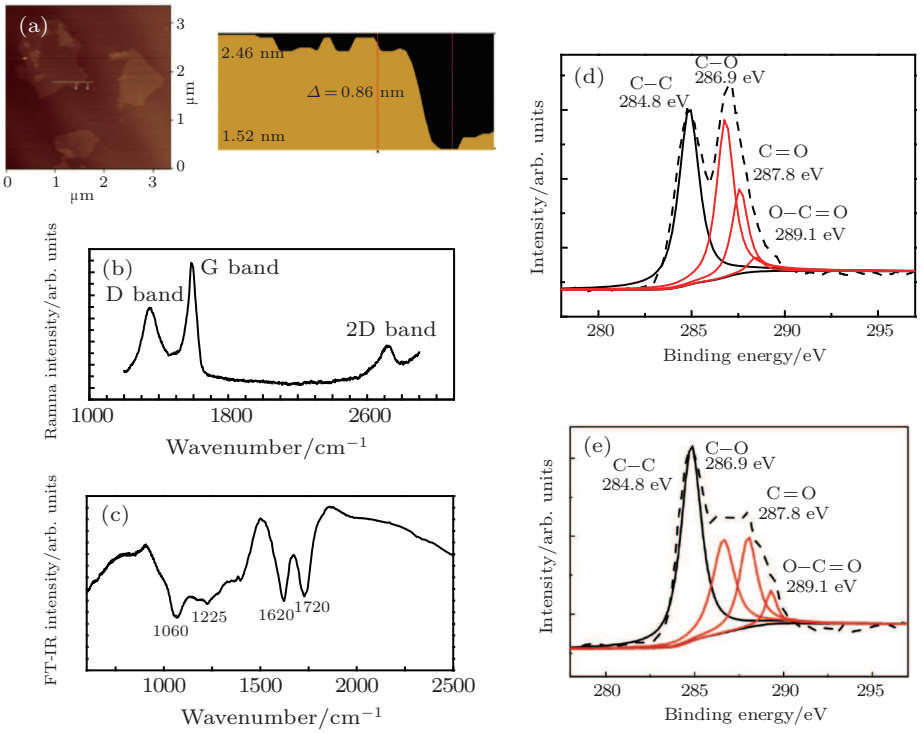


Fig. 1. (color online) AFM image of GO, the height difference between the two arrows is 0.86 nm (a). Raman spectrum (b) and FT-IR spectrum (c) of GO, indicate its lattice situation and the surface oxygenic functional groups. XPS images before (d) and after (e) the reduction, the plots are deconvoluted into four peaks corresponding to C=C/C–C in aromatic rings, C–O (epoxy and alkoxy), C=O and O–C=O groups, respectively.

3.2. Characterization of rGO–AuNP

Figure 2(a) shows SEM image of rGO–AuNP. It can be seen from the figure that AuNP grains are uniformly dispersed on the surface of rGO, most of which are attached to the sides or edges of sheets. The co-existences of Au, C, and O element in rGO–AuNP can be confirmed by EDS (See Appendix A Fig. S1) and XPS (Fig. 2(b)). From the above result it can be concluded that rGO–AuNP nano-composites are obtained. It is known that the chemical reactivity of geometrically strained regions in graphene lattices is much higher than those in other regions due to the destruction of sp^2,[33] and that electron density can be more easily displaced from the upper plane of the ring.[34] Therefore, the mechanism of *in-situ* synthesis of rGO–AuNP can be suggested as follows (Fig. 2(c)). Under the effect of electrostatic interaction and electrophilic substitution, Au^{3+} has a strong interaction with π orbitals of alkenes. With the anchoring and crystallizing of gold atoms on GO sheets, the seeds grow into nanoparticles gradually.

3.3. Size effect of AuNPs in rGO–AuNP-luminon–H_2O_2 CL system

The reaction of luminol with hydrogen peroxide in alkaline solution in the absence of a catalyst underwent weak CL. It is assumed that the catalyst AuNP may interact with the reactants or the intermediates of the reaction of luminol with hydrogen peroxide. Normally, the optimum pH range of the luminol reaction is between 10 and 11. For this novel rGO–AuNP-luminon–H_2O_2 CL system, different pH values are tested and shown in Fig. 3(a). The results show that the optimal pH environment for the CL system is 12.0, which is in agreement with that in the case of AuNP-luminon–H_2O_2 CL system.[35]

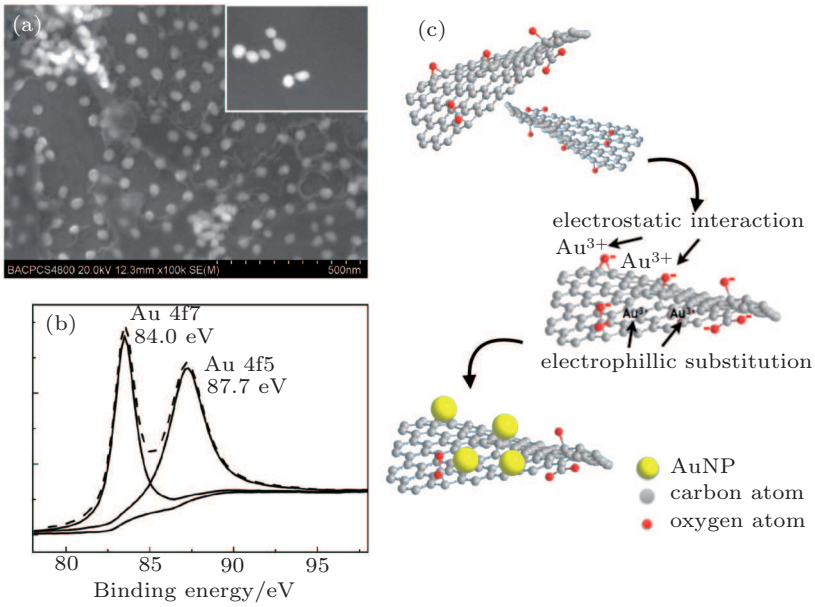


Fig. 2. (color online) SEM images of rGO–AuNP (a) and pure AuNP (in the inset) of the same nanoparticle size, XPS image of GO-AuNP nano-composites (b), and formation mechanism for the nano-composites (c).

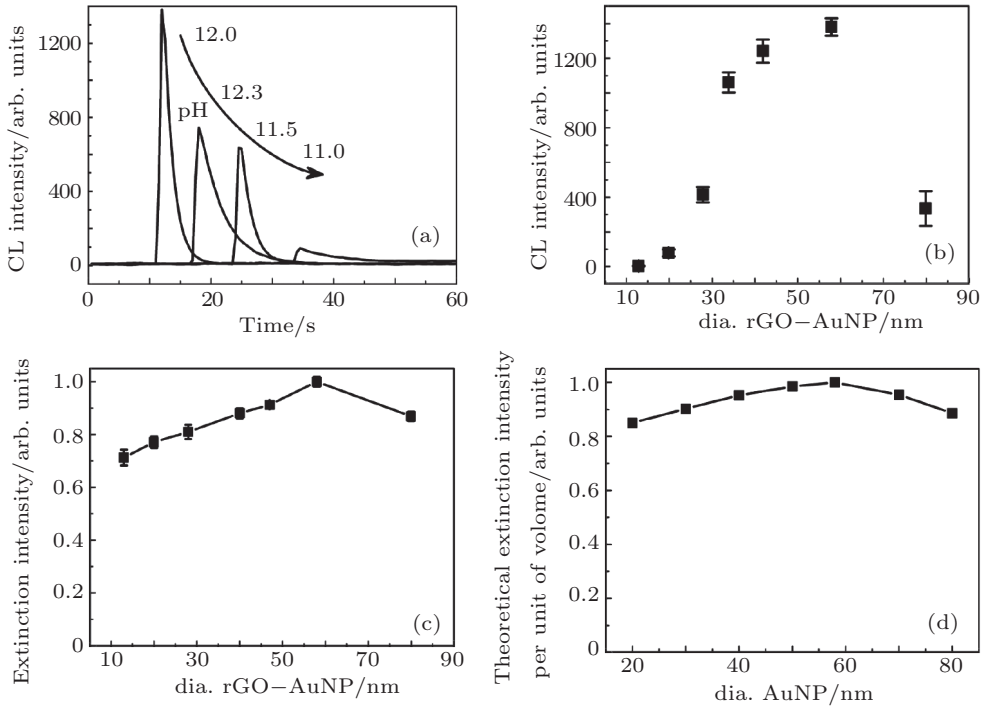


Fig. 3. Effects of pH on time-dependent CL intensity (a), and size effect on CL intensity of rGO–AuNP-luminon–H_2O_2 system (b). Experimental size effect on SPR intensity of rGO–AuNP (c), and theoretical size effect on SPR intensity (d). The calculated intensity is divided by the volume to obtain the intensity per unit volume of absorption.

Basically, the rate of heterogeneous catalysis increases with the available active surface area of catalysts.[35,36] Hence small-sized AuNPs are expected to give a higher rate of catalytic reaction due to their large surface-area-to-volume ratio. However, the adsorption of H_2O_2 onto the surfaces of nanoparticles would cause partial electron transfer from the particles to the adsorbed H_2O_2, which is known as particle-mediated electron transfer. The so-called particle-mediated electron transfer occurs in the too small NPs which may result in the adsorption of H_2O_2 molecules onto the surface of particle.[35] As a consequence, the catalytic activity of AuNPs is lowered with size decreasing. With the aim to obtain optimal size of AuNPs, size-dependent CL signals of rGO–AuNP-luminon–H_2O_2 CL system are recorded (Fig. 3(b)). It can be

seen that the 58-nm particles produce the most intensive CL signal. It is known that SPR intensity is considered to be an indicator of the electron density in the conduction bands of AuNPs.[37] The size-dependent absorption spectra (Fig. S2 of rGO–AuNP show that 58-nm AuNPs have the highest SPR absorption (Fig. 3(c)), which is consistent with the theoretic result of AuNPs calculated by 3D-FDTD method (Fig. 3(d)). Therefore, rGO–58-nm-AuNP is ultimately determined to be the optimal one for this CL system.

It should be noted that luminescence quenching occurs for very small particles. Figure S3 (Appendix A) shows that a weak enhanced CL signal appears after injection and the signal is stabilized at a low level, which is even lower than the starting intensity. After re-injection, the same phenomenon appears again. It can be concluded that the energy directly transfers from luminol to rGO–AuNP, due to the small separation of emitter-particle.

3.4. Assisted enhancement effect of rGO in rGO–AuNP-luminon–H_2O_2 CL system

In the presence of rGO, the CL signal of rGO–AuNP-luminon–H_2O_2 CL system is stronger than that of AuNP-luminon–H_2O_2 CL system (Fig. 4(a)). About 50% improvement is generally observed for each of all the samples. Such a significant improvement cannot be assigned to rGO itself, since it does not exhibit high catalytic activity unless it has a high concentration of luminal (200 μM).[38] In the present case of 2-μM luminol, CL signal of rGO is very weak in face (Appendix A: Fig. S4).

In order to research the role of rGO in rGO–AuNP-luminon–H_2O_2 CL system, conducting features of rGO–AuNP are characterized. In the high-frequency range of Nyquist plot, the rGO–AuNP modified glassy carbon electrode performs a smaller semicircle than AuNP modified electrode (Fig. 4(b)). The semicircle diameter of EIS is equal to the charge-transfer resistance (R_{ct}) at the electrode surface. The electrical conductivity and the electron transfer rate are improved in rGO–AuNP compared with those in AuNP. Moreover, EIS results provide clear evidence of large surface area of rGO–AuNP. In the lower frequency range, the Warburg impedance (corresponding to the evolution of Z'' as a function of the inverse of the square root of the frequency) of rGO–AuNP modified electrode is larger than the one of pure AuNP modified electrode. This phenomenon indicates that the double layer capacitance increases with the modified electrode, which corresponds to the larger surface area of gold NPs.

The increased electrical conductivity and surface area of rGO–AuNP thus justify the enhancement of CL signal. It is important to point out that the rGO–AuNP composites are rather stable. After a two-week storage, rGO–AuNP aqueous suspension has neither precipitate nor color change (Fig. 5), and 90% of CL signal can be still retained. The stability should be due to the platform of rGO, which immobilizes the AuNPs and isolates them from aggregation. In comparison, AuNPs alone will be agglomerated in aqueous two weeks later.

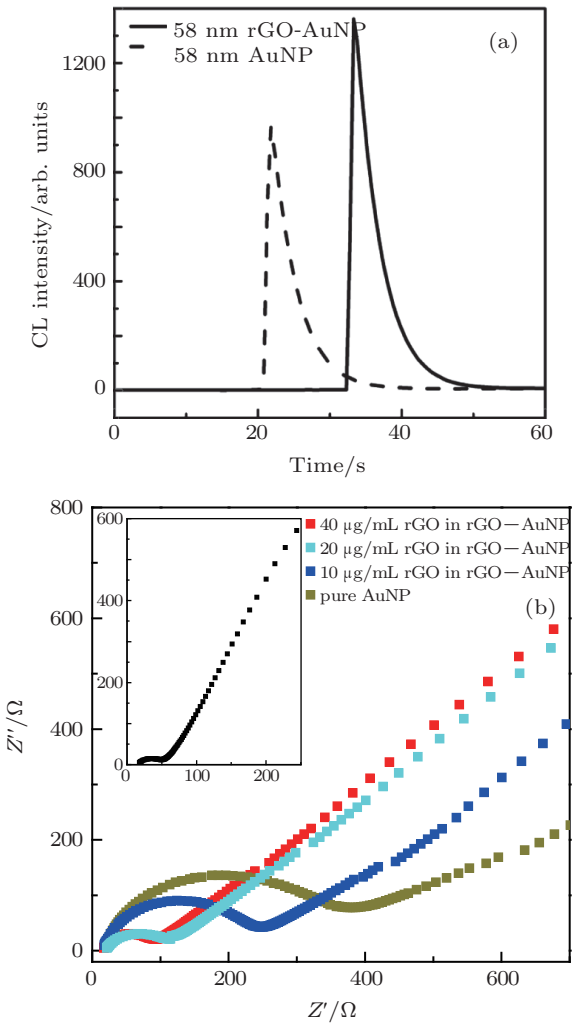


Fig. 4. (color online) Comparison of time-dependent CL intensity between pure AuNP and rGO–AuNP as catalyst on CL intensity (a). Nyquist plots obtained at GC electrode in 10-mM $K_3Fe(CN)_6$ and 1-M KCl. The frequency is in a range from 1 Hz to 100 kHz. The inset shows the Nyquist plot of pure rGO (b).

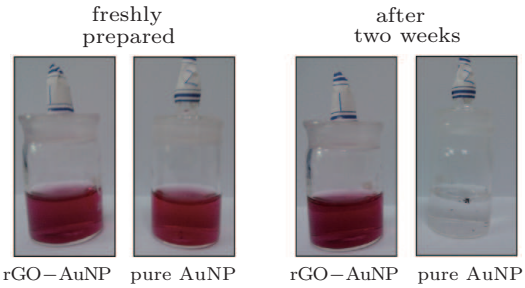


Fig. 5. (color online) Digital camera taken photographs of pure AuNP and rGO–AuNP.

3.5. Analytical applications of rGO–AuNP-luminon–H_2O_2 CL system

We evaluate the sensitivity of the proposed rGO–AuNP-luminon–H_2O_2 CL system to the hydrogen peroxide concentration. Effective CL signal can be obtained when the concentration of H_2O_2 varies from 0.4 mM to 250 mM. The plot of signal exhibits an excellent linearity in the concentration between 10 mM to 50 mM as shown in Fig. 6(a). When the concentration of H_2O_2 is beyond 50 mM, CL signal intensity decreases. That is mainly attributed to particle-mediated electron transfer.

RGO-AuNP provides the sites for the reaction between superoxide radical anion(O_2^-) from the dissociation of H_2O_2 and luminal (L^-), as illustrated in Fig. 6(b). As reported previously, metal NPs are very easy for some reducing groups involving NH_2, OH, SH, etc. to react with the oxygen-containing radicals and compete for the O_2^- CL needed by luminal radicals, resulting in the reduction of CL intensity.[35,39] The rGO–AuNP-luminon–H_2O_2 CL system has the promising potential for detecting the organic compounds containing NH_2, OH, SH groups. The influence of several compounds on CL signal intensity of the system is shown in Table 1. The quenching effect is clearly visible in the compounds containing NH_2, OH or SH, while inorganic substances (such as NaCl and KCl) have almost no effect on the system.

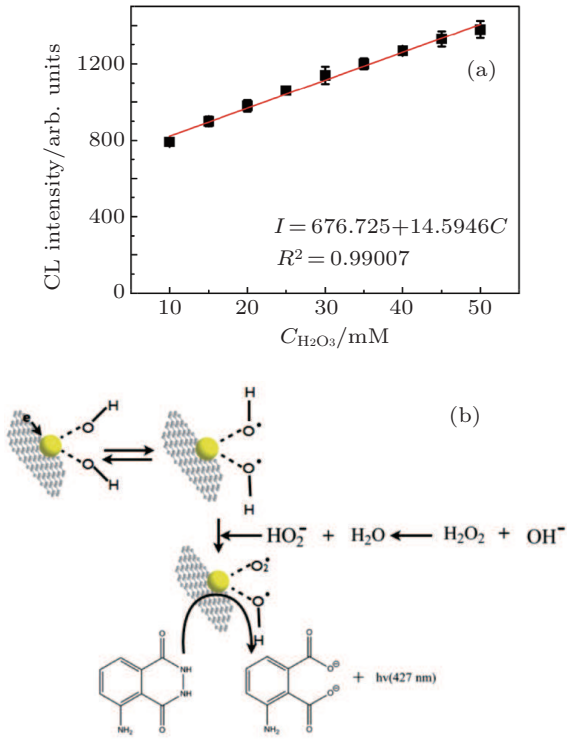


Fig. 6. (color online) Plot of CL intensity of H_2O_2 versus its concentrations (a); and schematic summary of possible chemiluminescence reaction mechanism involved in the examined system (b).

Table 1. Inhibition effects of chemical compounds (5×10^{-4} M) on rGO–AuNP-luminon–H_2O_2 CL system.

Chemical compounds	Blank (I_0)	Alanine	Glutamic acid	Tryptophan	Glutathione	Ascorbic acid	Sodium chloride	Potassium chloride
CL intensities (I)[a]	1380	1213	1297	1097	124	155	1401	1366
Quenching (I/I_0)	1	0.879	0.9399	0.7949	0.0899	0.1123	~ 1	~ 1

[a]The CL signals obtained by rGO–58-nm-AuNP-luminon–H_2O_2 system, in the case of pH value equal to 12.0. The concentration of luminal is 2 μM, and the concentration of H_2O_2 is 50 mM.

We therefore deem that the rGO–AuNP-luminon–H_2O_2 CL system has great practical potential in developing new CL sensors for various organic compounds when being combined with separation techniques such as high performance liquid chromatography and capillary electrophoresis. Furthermore, the rGO–AuNP nano-composites provide a promising approach to biological analysis, detection and immunoassays areas due to its good stability.

4. Conclusions

In this work, the novel rGO–AuNP nano-composites are prepared to improve the CL performance of luminol system. The nanocomposite is comprised of a single layer of rGO and in-situ prepared AuNPs. The size effect of particle and the assisted enhancement effect of rGO are studied and discussed in detail. The CL enhancement of rGO–AuNP is considered to be due to the large surface area and electron-transfer processe on nano-composites surface. RGO-58-nm-AuNP shows the strongest CL signal because of proper electronic structures, optimal surface area, and high electron density in the conduction bands. By means of the optimized rGO–AuNP-luminon–H_2O_2 CL system, hydrogen peroxide and many organic compounds containing amino, hydroxyl or thiol groups could be detected more precisely. The significance of this work is to provide the rGO–AuNP–luminon–H_2O_2 CL system, which is very promising for detecting many organic compounds.

Appendix A: Electronic supplementary information (ESI) available: [Figs. S1–S4]

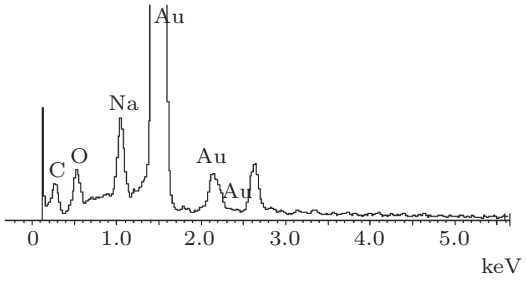


Fig. S1. EDS spectrum of rGO–AuNP, indicates the existence of Au, C, and O element in the rGO–AuNP nanocomposites.

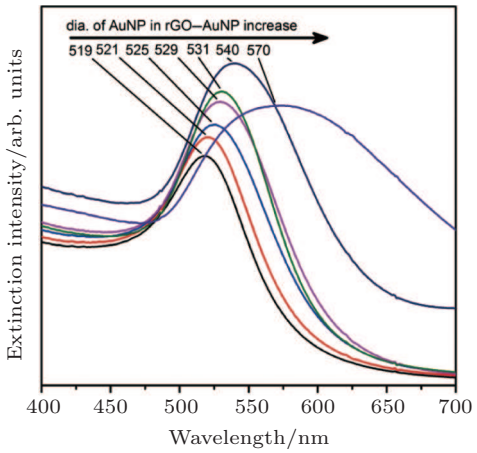


Fig. S2. (color online) Absorption spectra of various sizes rGO–AuNP nano-composites (a).

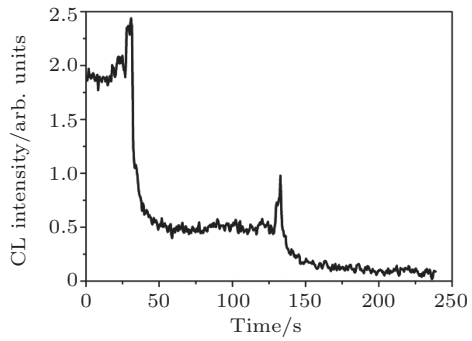


Fig. S3. CL spectrum of 13-nm rGO–AuNP nano-composites, two injections occurred in 30 s and 130 s.

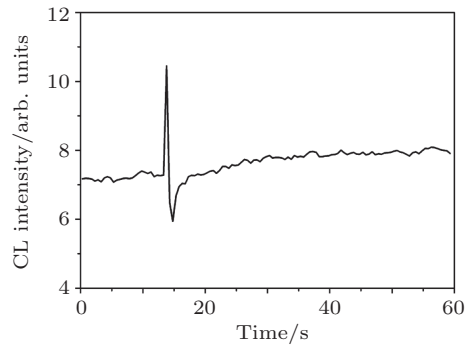


Fig. S4. CL spectra of luminon–H_2O_2 catalyzed by rGO. The concentration of luminol is 2 μM, and the concentration of H_2O_2 is 50 mM.

References

[1] White E H and Harding M J C 1964 *J. Am. Chem. Soc.* **86** 5686

[2] Isacsson U and Wettermark G 1974 *Anal. Chim. Acta* **68** 339

[3] Edwards J, Sprung R, Sprague R and Spence D 2001 *Analyst.* **126** 1257

[4] Pérez-Ruiz T, Martínez-Lozano C, Tomás V and Martín J 2003 *Anal. Bioanal. Chem.* **377** 189

[5] Marquette C A and Blum L J 2006 *Anal. Bioanal. Chem.* **385** 546

[6] Guo J Z, Cui H, Zhou W and Wang W 2008 *J. Photoch. Photobio. A* **193** 89

[7] Leff D V, Brandt L and Heath J R 1996 *Langmuir* **12** 4723

[8] Sastry M, Kumar A and Mukherjee P 2001 *Colloid. Surface A* **181** 255

[9] Safavi A, Absalan G and Bamdad F 2008 *Anal. Chim. Acta* **610** 243

[10] Bi S, Yan Y, Yang X and Zhang S 2009 *Chem-Eur. J.* **15** 4704

[11] Xiang Y J, Wu X C, Liu D F, Zhang Z X, Song L, Zhao X W, Liu L F, Luo S D, Ma W J, Shen J, Zhou W Y, Zhou J J, Wang C Y and Wang G 2006 *Chin. Phys.* **15** 2080

[12] Wang W S, He D W, Duan J H, Wang S F, Peng H S, Wu H P, Fu M, Wang Y S and Zhang X Q 2013 *Chem. Phys. Lett.* **582** 119

[13] Duan J H, He D W, Wang W S, Liu Y C, Wu H P, Wang Y S and Fu M 2013 *Chem. Phys. Lett.* **574** 83

[14] Tian D, Duan C, Wang W and Cui H 2010 *Biosens. Bioelectron.* **25** 2290

[15] Li Q, Liu F, Lu C and Lin J M 2011 *J. Phys. Chem. C* **115** 10964

[16] Dreyer D R, Park S, Bielawski C W and Ruoff R S 2010 *Chem. Soc. Rev.* **39** 228

[17] Schniepp H C, Li J L, McAllister M J, Sai H, Herrera-Alonso M, Adamson D H, Prud'homme R K, Car R, Saville D A and Aksay I A 2006 *J. Phys. Chem. B* **110** 8535

[18] Le Z G, Liu Z R, Qian Y and Wang C Y 2012 *Appl. Surf. Sci.* **258** 5348

[19] Xue Y, Zhao H, Wu Z, Li X, He Y and Yuan Z 2011 *Biosens. Bioelectron.* **29** 102

[20] Mao F, Zhang C, Zhang Y W and Zhang F S 2012 *Chin. Phys. Lett.* **29** 076101

[21] Deng P F, Lei T M, Lu J J, Liu F Y, Zhang Y M, Guo H, Zhang Y M, Wang Y H and Tang X Y 2013 *Chin. Phys. Lett.* **30** 018101

[22] Goncalves G, Marques P A A P, Granadeiro C M, Nogueira H I S, Singh M K and Grácio J 2009 *Chem. Mater.* **21** 4796

[23] Fu X, Bei F, Wang X, O'Brien S and Lombardi J R 2010 *Nanoscale* **2** 1461

[24] Lee Y H, Polavarapu L, Gao N, Yuan P and Xu Q H 2012 *Langmuir* **28** 321

[25] Hummers W S Jr and Offeman R E 1958 *J. Am. Chem. Soc.* **80** 1339

[26] Park S and Ruoff R S 2009 *Nat. Nanotechnol.* **4** 217

[27] Sun Z, Yan Z, Yao J, Beitler E, Zhu Y and Tour J M 2010 *Nature* **468** 549

[28] Wu P, Shao Q, Hu Y, Jin J, Yin Y and Zhang H 2010 *Electrochim. Acta* **55** 8606

[29] Zhang J, Yang H, Shen G, Cheng P, Zhang J and Guo S 2010 *Chem. Commun.* **46** 1112

[30] Suo S, Wen D, Zhai Y, Dong S and Wang E 2010 *ACS Nano* **4** 3959

[31] Han J, Zhuo Y, Y Q Chai, Mao L, Yuan Y L and Yuan R 2011 *Talanta* **85** 130

[32] Mao Y, Bao Y, Wang W, Li Z, Li F and Niu L Niu 2011 *Talanta* **85** 2106

[33] Loh K P, Bao Q, Ang P K and Yang J 2010 *J. Mater. Chem.* **20** 2277

[34] Kuila T, Bose S, Mishra A K, Khanra P, Kim N H and Lee J H 2012 *Prog. Mater. Sci.* **57** 1061

[35] Zhang Z F, Cui H, Lai C Z and Liu L J 2005 *Anal. Chem.* **77** 3324

[36] Sharma R K, Sharma P and Maitra A 2003 *J. Collid Interf. Sci.* **265** 134

[37] Henglein A 1993 *J. Phys. Chem.* **97** 5457

[38] Wang D M, Zhang Y, Zheng L L, Yang X X, Wang Y and Huang C Z 2012 *J. Phys. Chem. C* **116** 21622

[39] Wang L, Yang P, Li Y, Chen H, Li M and Luo F 2007 *Talanta* **72** 1066